Pattern Formation Fueled by Dissipation of Chemical Energy: Conclusive Evidence for the Formation of a Convective Torus 1

ARTICLE *in* THE JOURNAL OF PHYSICAL CHEMISTRY A · JANUARY 2002

Impact Factor: 2.69 · DOI: 10.1021/jp012502k

2 AUTHORS, INCLUDING:

Reuben H Simoyi
Portland State University
117 PUBLICATIONS **1,833** CITATIONS

Pattern Formation Fueled by Dissipation of Chemical Energy: Conclusive Evidence for the Formation of a Convective Torus[1]

Bice S. Martincigh

Department of Chemistry and Applied Chemistry, University of Natal, Private Bag X10, Dalbridge 4014, Republic of South Africa

Reuben H. Simoyi*

Center for Nonlinear Science and the Department of Chemistry, West Virginia University, Morgantown, West Virginia 26506-6045

Received: July 2, 2001; In Final Form: October 23, 2001

An exothermic, autocatalytic chemical reaction can produce a lateral instability which can result in a rapidly moving wave of chemical reactivity. The propagating wave is strongly influenced by thermocapillary effects. At high Marangoni numbers the traveling wave has shown irregular patterning and spatiotemporal irregularity that is aligned in the direction of wave propagation. At lower Marangoni numbers effective coupling occurs between thermocapilary and thermogravitational Rayleigh−Benard type effects. This coupling has produced powerful thermal plumes just behind the leading wave front as well as a series of concentric patterning that represent "transient" Turing patterns. Observations of these effects had led to the conjecture that the wave forms a series of convective tori as it propagates. In this paper recent experimental data are produced that clearly show the dynamic formation of convective tori at the wave front.

Introduction

The first theory of the chemical basis of morphogenesis was proposed by Turing in 1952 when he suggested that spontaneous symmetry-breaking bifurcations can occur from a homogeneous state due to a coupling of nonlinear chemical kinetics and diffusion.[2] Such diffusion-reaction systems can be represented by the model

$$\delta u/\delta t = D\nabla^2 u + F(u) \tag{1}$$

where u is the vector of state variables, D is the matrix of diffusion coefficients, and $F(u)$ is the nonlinear function representing chemical kinetics. A simple solution of a two-variable model of eq 1 using Dirichlet boundary conditions gives spatiotemporal patterning if the length scale of the fast-reacting activator, $[D_{11}/a_1]^{1/2}$, is shorter than that of the slow-reacting inhibitor, $[D_{22}/a_2]^{1/2}$, where a_1 and a_2 are the pseudo-first-order growth rate constants. Patterns should develop with a chemical wavenumber, q_0, of[3]

$$q_0 = {}^1/_2[a_2/D_{22} - a_1/D_{11}]^{1/2} \tag{2}$$

It has been, however, very difficult to produce Turing patterns according to eq 1. No experimental observations for Turing patterns from chemical systems were observed until the chlorite−iodide−malonic acid, CIMA, reaction reported by the Bordeaux group in 1990.[4]

Other chemical systems, however, which do not necessarily obey the preconditions for Turing patterns; e.g. nonisothermal or with one of the reactants immobilized, $D = 0$, have shown pattern formation. Among some examples of such systems are reactive gels surrounded by reactive fluids,[5] catalytic rings,[6] low-pressure reactions on a single crystal,[7] and electrochemical dissolution of nickel.[8] In all these cases, some global or nonlocal effects caused patterns to form. A typical global effect is heat generation, especially from exothermic chemical reactions.

Addition of heat, especially in fluid and in gaseous environments, to a system capable of generating Turing patterns can either completely annihilate them or stabilize them. For example, chemically driven convection generated by density gradients due to concentration variations of the Turing structures can stabilize Turing patterns in roll structures.[9] For fluid systems heated from below and with a freely deformable upper surface, the heat also introduces, apart from density gradients, extensive thermocapillary convection.[10]

Turing's model, according to eq 1, does not include convection. With convection, the resulting chemical gradients may lead to mass density gradients that should annihilate any emerging Turing patterns. Convection plays an important role in chemical wave propagation and should also determine the fate of Turing patterns.

The first experimental evidence of Turing patterns was observed in a polyacrylamide gel which was designed to stop fluid motion from convective instabilities.[4] Turing patterns have now been observed in liquids confined to capillary tubes.[11]

In this manuscript, we examine patterning generated in ungelled solutions containing an exothermic autocatalytic, bistable chemical reaction. Upon triggering of the reaction mixture using the autocatalyst, a chemical wave of reactivity is generated. The observed patterns are resident at the wave front and in the wake of the wave. Among some of the patterns generated were concentric patterns which could be sustained for several minutes before being destroyed by subsequent convective instabilities.[12] It was conjectured, then, that these concentric patterns were generated by the formation of a series

* Corresponding author. E-mail: arachsimoyi@michaelangelo.net.

10.1021/jp012502k CCC: $22.00
Published on Web 12/14/2001

of convective tori. Using special indicators, we report in this manuscript on conclusive visual evidence that a convective torus is formed which in turn forms the stripes that generate the observed patterns. A brief explanation of the forces responsible for this coherence is also given.

Chemical Reaction Mechanism

The dynamics reported in this paper are derived from the chlorite−thiourea and the chlorite−methylthiourea reactions.[13] The kinetics and mechanism of this reaction have been extensively studied.[14,15] Chlorite oxidizes thiourea and substituted thioureas under acidic or neutral pH conditions to give sulfate and ureas. The stoichiometry of the reaction in excess oxidant can be generalized on the basis of thiourea as follows:

$$2ClO_2^- + SC(NH_2)_2 + H_2O \rightarrow SO_4^{2-} + OC(NH_2)_2 + 2H^+ + 2Cl^- \quad (R1)$$

The reaction proceeds via consecutive 2-electron transfers from the sulfur atom to the chlorine center such that the series of thiourea oxides sulfenic, sulfinic, and sulfonic acids are formed at successive transfers:

$$ClO_2^- + SC(NH_2)_2 + H^+ \rightarrow HOCl + (NH_2)(NH)CSOH \quad (R2)$$

$$ClO_2^- + (NH_2)(NH)CSOH + H^+ \rightarrow HOCl + (NH_2)(NH)CSO_2H \quad (R3)$$

$$ClO_2^- + (NH_2)(NH)CSO_2H + H^+ \rightarrow HOCl + (NH_2)(NH)CSO_3H \quad (R4)$$

HOCl is a more powerful oxidizing agent and can perform the oxidations (R2)−(R4) much more efficiently than ClO_2^-. With excess chlorite in the reaction medium, the HOCl formed from the reduction of chlorite reacts with excess ClO_2^- to give yellow ClO_2:[16,17]

$$HOCl + 2ClO_2^- + H^+ \rightarrow 2ClO_2(aq) + Cl^- + H_2O \quad (R5)$$

In the presence of reductant (thiourea and its oxidation intermediates), the ClO_2 formed in reaction R5 is quickly reduced back to ClO_2^-, HOCl, and Cl^-. However, ClO_2 is inert to the sulfonic acid (aminoiminomethanesulfonic acid as formed in reaction R4) and would only react with it very slowly. Thus, the appearance of chlorine dioxide is an indicator that all the thiourea has been oxidized to its sulfonic acid.

This reaction is autocatalytic and bistable in a continuously stirred tank reactor. The nonlinearity is generated by the positive feedback loop derived from the autocatalysis. HOCl is the autocatalytic species, and the reaction can be triggered by addition of a small drop of HOCl solution (or chlorine water). In terms of single-step mechanisms, HOCl autocatalysis can be explained via the asymmetric intermediate Cl_2O_2[18,19]

$$ClO_2^- + HOCl + H^+ \rightarrow Cl_2O_2 + H_2O \quad (R6)$$

followed by

$$Cl_2O_2 + 2H^+ + 2e^- \rightarrow 2HOCl \quad (R7)$$

The reductant, represented by $2e^-$, can be any of the reducing sulfur species in solution. Addition of reactions R6 and R7 will show that for every 1 mol of HOCl formed in reactions R2−R4, 2 mol is formed after each further oxidation. This is the basis for quadratic autocatalysis. We would expect a rapid increase in the rate of reaction with time, and this would include reaction R5 which forms chlorine dioxide. The reaction displays typical clock reaction characteristics in which there is an initial quiescent period followed by a rapid formation of chlorine dioxide. The formation of chlorine dioxide is accompanied by a very large release of heat.[17] The heat generated is a very important parameter in wave propagation. The heat generates the convective instabilities that help fuel the propagation of the wave.

In these remarkable sets of reactions, four separate events happen very rapidly at the end of the induction period. We have mentioned heat generation and chlorine dioxide formation above, with the other two events being the rapid formation of sulfate and an equally rapid formation of acid. All these four events can be used to follow the wave propagation. While the sulfenic and sulfinic acids are oxidized by ClO_2^-, HOCl, and ClO_2, the sulfonic acid will accumulate until there is enough HOCl (by the autocatalytic route) to cleave the C−S bond and form sulfate:

$$HOCl + (NH_2)(NH)CSO_3H + H_2O \rightarrow SO_4^{2-} + OC(NH_2)_2 + Cl^- + 3H^+ \quad (R8)$$

Due to the autocatalytic nature of the production of HOCl, concomitantly, there will be autocatalytic formation of SO_4^{2-} and H^+. The wave front is characterized by a reaction zone of about 3 mm in width. Though all four events occur at about the same time, the sequence is as follows: acid front followed by sulfate, then chlorine dioxide, and finally heat.

Experimental Section

Materials. The following analytical grade reagents were used without further purification: thiourea, methylthiourea, barium chloride (Aldrich); perchloric acid 70−72%, soluble starch, methyl red, methyl orange (Fisher). Sodium chlorite is sold in its technical grade form (about 80%). A single recrystalization (ethanol−water mixture) brought the assay to 95%. The analysis of sodium chlorite was performed iodometrically by adding excess acidified iodide and titrating the liberated iodine against standard thiosulfate with freshly prepared starch as indicator.[20] Stock solutions of sodium chlorite were prepared fresh for each set of experiments and stabilized with 0.001 M sodium hydroxide[21] if the experiments were going to be run in high-acid environments. The sodium chlorite solutions were also stored in dark winchester vessels wrapped in aluminum foil to reduce decomposition by light.

Methods. The chlorite, thiourea, acid, and/or indicator were thoroughly mixed before being poured into the reaction vessel. Chlorite was added last by a rapid delivery pipet. The wave could self-initiate, but the induction times for clocking were stochastic. The time taken before clocking was very important in determining wave dynamics especially velocity and shape. For example, solutions that clocked early gave a faster-moving wave front from the point in initial perturbation.

After solutions were thoroughly mixed, they were allowed to settle until all physical ripples disappeared and were triggered by the addition of a 0.05 mL micropipet drop of a solution containing HOCl.

Image Analysis. Video Imaging experiments were useful for studying the wave velocities, the structure of the propagating wave front, and the spatiotemporal patterns. All experiments were recorded using a PULNIX TMC 74 color camera attached

to a Sony PVM-1334Q RGB monitor and a Panasonic AG-1960 professional video cassette recorder. The video cassette recorder and the RGB monitor were also interfaced to a Pentium III computer via a PCVision Plus frame grabber model PFGPlus-640-3-60 capable of storing a 640 × 480 square pixels image. Image analysis was via Bioscan Optimas version 6.0 software. The recorded experiments were played back on the video cassette and the desired frames captured and stored as JPEG files. The velocities were measured using the motion analysis macro of the Bioscan software which uses Microsoft Excel 4.0 for the statistical analysis. Further processing of the acquired images included noise and color filtering.

Reaction Energetics

The chlorite−thiourea reaction is extremely exothermic, and our rough measurements suggest an enthalpy change of −1169 kJ mol^{-1}. Since enthalpy change is an extensive property, the heat generated can be controlled by initial reagent concentrations. The exotic dynamics we report here are obtained within a small range of initial concentrations that allow the thermogravitational and thermocapillary forces to couple sufficiently enough to produce organizational coherence. Initial concentrations used were such that $[ClO_2^-]_0/[SC(NH_2)_2]_0 \geq 2$. A ratio above 2 ensured the formation of chlorine dioxide and sulfate. Batch experiments showed that, with the reagent concentrations $[ClO_2^-]_0 = 0.0004$ M and $[SC(NH_2)_2]_0 = 0.0002$ M, the increase in temperature of the reagent solutions was approximately 3 °C. Most of the data reported here were obtained for ΔT between 2.8 and 4.5 °C. The reactants are mostly organic reagents (thiourea), and the products are inorganic (sulfate). Our experimental data gave an isothermal density change, $\Delta\rho$, of 2.7×10^{-3} g cm^{-3}. Products are thus heavier than the reactants (at same temperature conditions).

Rayleigh−Benard Convection. Thermogravitational forces of the Rayleigh−Benard-type can be assessed in isolation in a tube which has a relatively small surface area exposed to the atmosphere. One can easily make the prediction that if the wave is ascending in a tube, then the wave front will be stable and a planar front should emerge. The wild card is the temperature change. Density will always decrease with increasing temperature, and one has to assess whether the value of ΔT between 2.8 and 4.5 °C is sufficient to offset the isothermal density change and cause a flip-flop in the densities of the reacted and unreacted solutions. However, with an ascending wave, any approach to thermal equilibrium at the wave front will stabilize the front. That is, any deformity in the wave front to induce fingering into the unreacted region will result in a fast thermal equilibrium in the fingering region with the result that the finger will become heavier than the surrounding solution and fall back into the reacted region. Only experimental work will determine the shape of the wave front for descending waves (in a tube). Again, thermal expansion needs to be coupled to the isothermal density change for any meaningful structures to occur. A large increase in one effect will result in poor coupling, giving rise to structureless wave propagation.

For waves propagating in a Petri dish or in an unbound $x-y$ plane, we can make valid predictions as to the general shape of the wave front based upon the forces we expect to be at play at the wave front and behind it. Figure 1 shows a schematic diagram of a generic wave front. Since the solutions are open to the atmosphere, apart from evaporative cooling, we expect extensive thermocapillary convection. Table 1 gives the surface tension data which is relevant to our reaction solutions. These were measured by a combination of the Du Nouy tensiometer and capillary rise methods.[22] It was difficult to thermostat the film for Du Nouy methods, and thus higher temperatures were measured by the capillary rise method.

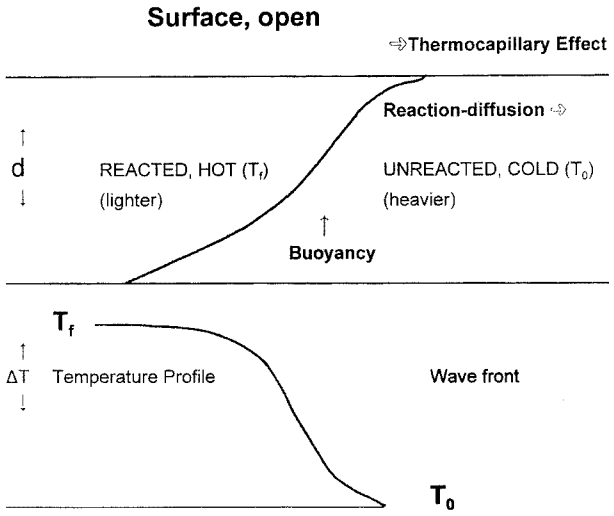

Figure 1. Schematic diagram showing the forces involved in a traveling wave from an exothermic autocatalytic chemical reaction. The highest temperature, as shown in the lower scale, is located in the bulk of the reacting solution. The width of reaction zone is approximately 3 mm. At high values of ΔT, thermocapillary effects are dominant over the thermogravitational forces.

TABLE 1: Effect of Temperature on Surface Tension[a]

temp/K	$10^{-3}\sigma$/N m^{-1}
Reactant Solution	
298	72.58
Product Solution	
298	72.42
303	71.99
308	71.50
313	70.92

[a] $\delta\sigma/\delta T = -9.5 \times 10^{-5}$ N m^{-1} K^{-1}.

Marangoni Convection. Surface tension will always decrease with temperature, and so the exothermicity of the reaction should fuel a powerful force acting in concert with the wave propagation motion (see Figure 1 showing direction of reaction−diffusion forces as well as thermocapillary convection). The interesting feature of our data is that, at 298 K, the reactant solution's surface tension is larger than the product solution's. This would mean that, even in the absence of a temperature jump, there will still exist a strong surface tension effect in the same direction as the reaction−diffusion force. Buoyancy effects will exist due to the elevated temperature of the reacted (and reacting) solutions, and hence, one will observe the "sliding over" effect of the hot reacted matter over the cold, unreacted material. The incentive at the top to move faster is enhanced by surface tension which does not exist in the bulk of the solution. What follows in this manuscript is the interplay between surface tension, fingering, and pluming which will give the coherence that manifests itself, to us, as concentric patterning and Turing-like structures. The only way a convective torus can be formed is if extensive fingering occurs, which, at some point, turns into a plume to complete the torus.

Results

Tube experiments gave the first evidence that the autocatalytic oxidation of an organic sulfur compound could deliver double-diffusive convection. By adjustment of the initial concentrations

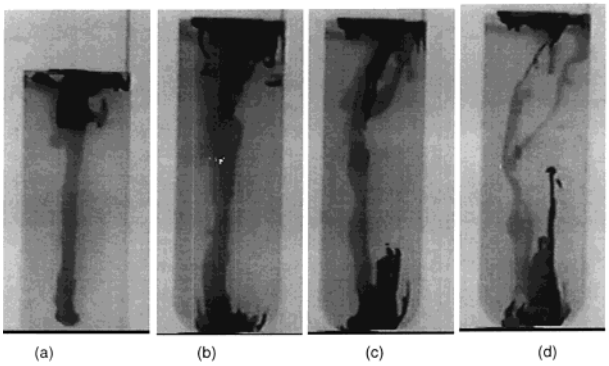

Figure 2. Extensive fingering observed in the chlorite−methythiourea reaction with 5% starch as indicator. The finger in (a), upon reaching the bottom of the vessel, rises to become a plume in (b)−(d). Note that, in (c) and (d), the plume rises in a region away from the path of the finger due to availability of reagents.

of chlorite and thiourea, an exothermic temperature increase of between 2.8 and 4.5 °C could be maintained between the reacted and unreacted reaction solutions. This temperature range displayed the most fascinating dynamics. Outside of this range structureless wave propagation was observed. The appropriate ratios of chlorite and thiourea were rapidly mixed and poured into the tube. Reagent solutions were first degassed with argon to remove oxygen. Uninitiated wave propagation always started from the top. Wave fronts could be followed by the yellow chlorine dioxide color. However, the color was too faint to be able to deliver sharply defined fronts and had to be enhanced by the use of indicators. The chemistry of the waves indicates that the foremost front of the wave is defined by a sharp pH change.[17] Directly behind the pH front is rapid formation of sulfate and a chlorine dioxide wave followed behind the sulfate. The chlorine dioxide wave front was also slightly ahead of a heat front where, within a small >3 mm region, the temperature increased by 2.8 to 4.5 °C depending on initial conditions. All four fronts were experimentally measured and detected. Thermocouples were used to measure temperature gradients.

Descending waves propagated with structure, while ascending waves were planar. At isothermal conditions, the products (sulfate and other inorganic salts) are heavier than the reactants (organic sulfur compounds). However, the temperature increase of the products was just sufficient to alter the density of the products such that they temporarily became lighter than the reactant (unreacted) solutions. Approach of thermal equilibrium then reversed the situation. To illustrate this effect, a 5% starch solution was used as the indicator. Starch solutions with mercuric iodide gave a deep blue complex with chlorine dioxide. Starch also significantly increased the viscosity of the medium and reduced the mobility of the reactants. Front velocities were greatly reduced. While, in general, heat conduction is at least 100× faster than diffusion, addition of starch accentuated this effect to the point that any defect along the wave front was quickly magnified by a combination of heat conduction and diffusion. Any finger of reacted material extending into the unreacted region will quickly lose heat and become heavier, thus producing extensive salt fingering.[23] The pictures shown in Figure 2 show such fingering patterns for a descending wave. If we continue to follow this finger, as the series in Figure 2 shows, upon reaching the bottom of the vessel, the finger becomes a plume and rises. The mechanism involved in such a process is explained later in this manuscript. Without a plume, a convective torus cannot be formed by a finger alone.

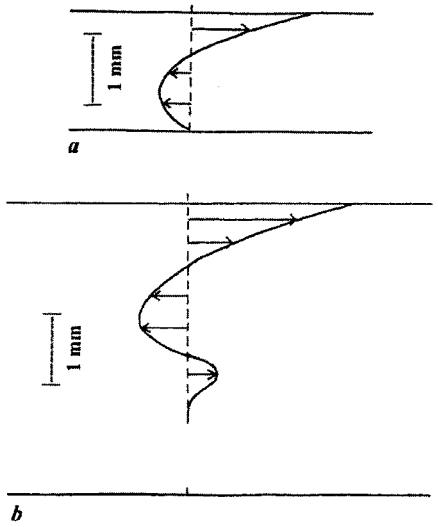

Figure 3. (a) Observed wave profile in shallow layers. For aqueous environments depths between 1.1 and 3.3 mm generated such global flow. For pure hydrothermal waves, the flow curve shown above can be modeled according to the equation for hydrothermal waves: $v_x = h(h - 2/3)$, where h is the normalized depth of the solution and v_x is the horizontal wave velocity. (b) Flow profile observed in deeper solutions. The bulk solution is unaffected by the wave motion above. The bottom layers are finally triggered by extensive fingering from the reacted solution above.

Buoyancy effects such as represented by fingering patterns and plumes, on their own, are insufficient to produce three-dimensional patterning. There should exist a force in the horizontal plane which can effectively couple with the vertical buoyancy forces. Petri dish experiments had shown the existence of a very strong horizontal force which gave a lateral instability which delivered a rapidly moving wave front.[24] Shallow layers of depth less than 3.3 mm gave traveling waves that propagated while leaving a well-defined structure in their wake.[25] This was evident through the use of barium chloride as an indicator. The deposition of barium sulfate in the wake of the wave mimicked the hydrodynamic motion. Without barium chloride, the same hydrodynamic motion could be observed by the use of polystyrene beads which were observed under a microscope.[26] The basic flow structure was as that derived from pure hydrothermal waves without chemical reaction. The rapidly moving upper layer of the solution was counterbalanced by a return flow at the bottom (Figure 3a).[27]

The spatiotemporal patterning generated in the wake of the wave, however, was heavily dependent on the solution depth, the viscosity of the medium, the geometry of the vessel, and the initial reagent concentrations.

Solution Depth. The fascinating convective tori reported here were derived from solutions of depths between 1.7 and 3.3 mm. In a previous publication we reported that deep solutions delivered incoherent and very transient patterning in which the traveling wave only involved the top part of the solution with the deeper layers unaffected (Figure 3b).[25] The lower layers were later triggered by extensive fingering. Deeper solutions had stronger buoyancy forces which annihilated any emerging patterns. Shallow or thin layers, on the other hand, had negligible buoyancy forces along the perpendicular z axis, resulting in a structureless wave propagation. The 1.7−3.3 mm depth had the correct coupling of buoyancy and thermocapillary forces, resulting in coherent patterning.

Viscosity of the Medium. Starch, being a very complex molecule, greatly increases the viscosity of the reaction medium.

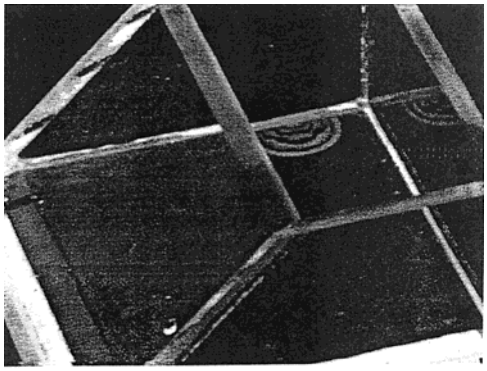

Figure 4. Type of concentric patterning observed as the wave propagates outward from the point of an initial perturbation. Four circular bands of precipitation, separated by regions of null precipitation, can be seen. $[ClO_2^-]_0 = 0.00225$ M, and $[SC(NH_2)_2]_0 = 0.0113$ M.

The higher viscosity reduces the wave propagation velocity as well hydrodynamic turbulence. Much more extensive fingering is observed with starch than without (Figure 2). In a Petri dish, starch produces beautiful three-dimensional patterns which we showed in a previous publication.[11] Without starch, the patterns are less complex.

Geometry of the Vessel. Spatiotemporal patterning is generally determined by the shape of the reaction vessel. Free pattern formation is possible in an unbound $x-y$ plane which could not be generated in a Petri dish. Spatiotemporal patterning observed in a Petri dish generally mimicked the cylindrical geometry of the vessel.[28] We assumed an unbound $x-y$ plane for waves initiated from the center of a vessel of dimensions of at least 10 cm square.

Reagent Concentrations. A complete reaction, in which the sulfur center of the thiourea is completely oxidized to sulfate, requires a 2:1 ratio of chlorite to thiourea.[9] Thus, at least this ratio was maintained for all reactions. A ratio greater than 2 delivered extraneous heat from the pure oxyhalogen reaction R2. This ClO_2^-/HOCl reaction with $R \gg 2$ also trailed the wave front quite considerably, thereby delivering a much wider heating zone. Concentrations in the range of 10^{-5} M delivered slow, structureless waves with homogeneous $BaSO_4$ precipitation and no spatiotemporal patterning in the wake of the wave.[26,27] High concentrations of 10^{-3} M and higher delivered very rapidly propagating waves with precipitation patterning aligned in the direction of wave propagation. Concentrations of about 10^{-4} M were suitable for the generation of the observed Turing-like patterns.

Enthalpy is an extensive property, and so higher concentrations gave out more heat which generated a higher Marangoni effect.[29] Since the thermocapillary effects act only in the horizontal direction, higher Marangoni numbers deliver greater lateral velocities. Buoyancy forces (in the z direction) at this time scale do not couple well with the Marangoni effect and are negligible in shallow solution layers.

Observation of Turing-like Structures. The theme of this manuscript is the observation of a convective torus. These were evident from the observation of bands of alternating null and full precipitation of $BaSO_4$ as the wave propagates from the position of an initial perturbation (Figure 4). Our first initial dubbing of this banding as arising from successive formations of convective tori was a mere conjecture with no proof. In general, without gelling to avoid hydrodynamic instabilities, it is difficult to generate coherent patterning in aqueous solutions. Convective instabilities actively work to destroy any coherence generated by the reacting solution. Remarkably, the observed

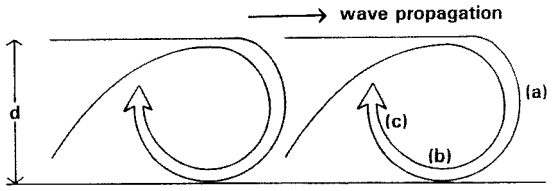

Figure 5. Schematic diagram showing the formation of thermal plumes behind the wave front. This happens with slower moving wave fronts where there is no clear separation between convective rolls. (a) represents fingering, (b) represents back flow, and (c) represents a plume.

concentric precipitation patterns can survive for periods up to 3 min before being destroyed by the hydrodynamic motion in the wake of the wave. The general pattern of wave propagation consists of a rapidly accelerating wave before it attains a constant high velocity. This is the region (with the accelerating wave) where there is adequate coupling between buoyancy and thermocapillary forces. A previous study established that lateral velocities were directly proportional to the surface tension gradient.[29] This gradient is set up by temperature, concentrations, and composition. The temperature effect is dominant, and as with all autocatalytic reactions, the rapid increase (sigmoidal) in reaction rate concomitantly increases the heat generation which, as in a domino effect, will increase the surface tension gradient and subsequently the lateral velocity.[12] Thermal runaway is only avoided by the diffusion of reactants into the reaction zone, which finally results in a constant wave velocity. In the region where the wave attains a constant velocity we observed well-defined (thermal) plumes just behind the leading wave front. Their generation and origin have been adequately explained elsewhere[29] and seem to involve overlapping convective tori. Figure 5 is a schematic sketch of what happens in the situation of overlapping convective tori. There will be no clear separation between successive convective rolls. Forces labeled a, b, and c in the figure indicate respectively fingering, back flow, and pluming. Slower wave propagation velocities can give rise to the situation shown in Figure 5. Faster wave propagation will produce spatially separated convective rolls. These nonoverlapping convective tori can give the observed bands of Turing-like structure at the onset of wave propagation.

Visual Evidence for a Convective Torus. The best way to study hydrodynamic motion in the region of concentric precipitation patterns is to study a two-dimensional projection of the $x-z$ plane of Figure 4. An approximation of such a projection can be effected by the use of a long, narrow rectangular trough in which the reaction will be observed. The typical vessels used were 300 mm long by 10 mm deep with widths varying between 3 and 5 mm. The vessels were made of plexiglass to avoid spurious wave initiations as had been observed with quartz vessels.[16] After pouring the reactant solution into the vessel to the desired depth, the wave was initiated from the side by addition of a 0.05 mL drop of dilute HOCl. The wave propagation was then followed from the side and from the top by a CCD camera interfaced to a computer. With methyl orange indicator, the acidic wave front could be followed.

The initial data which led us to the conclusion that the chemical system was generating repeating structures on a length scale came from the observation of what we called the "sawtooth effect".[29] These were observed in deep solutions in which fingering never reached the bottom of the solution for each convective roll. The flow structure is shown in Figure 3b. Thus, in deeper solutions, the wave propagated with a periodic pattern

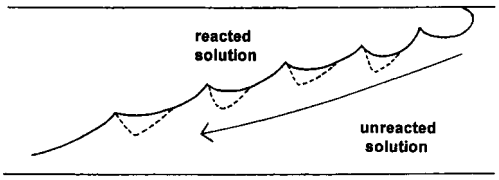

Figure 6. Saw-tooth effect. This is the shape of the wave in a long narrow rectangular and deep vessel. Each periodic variation represents a convective roll. The bottom of the wave is under constant back flow, and the wave front oscillates between the solid and dashed lines.

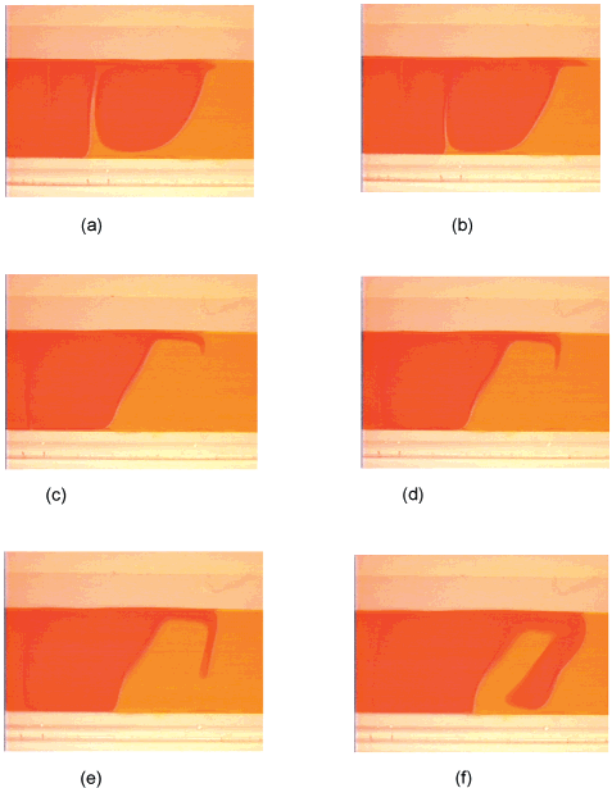

Figure 7. Visual evidence for the formation of a convective torus. Methyl orange was used as the indicator. The rapid formation of the wave at the surface is fueled by the Marangoni effect. Movement of the leading wave front down into the bulk unreacted solution is due to standard thermogravitational effects The bending of the wave front backward to form a convective roll is due to the back flow resident at lower depths and necessary for mass balance. The solution depth used here of 5 mm is much larger than that used for experiments shown in Figure 4. The deeper solution used exaggerates the fingering effects. For shallower solutions, pluming can commence at (e).

that resembled the teeth of a saw (Figure 6). The lengths of these repeating structures and their periods were determined by the initial reagent concentrations. The teeth of the saw are inclined away from the wave propagation direction denoting that they are under the effect of a constant back flow. Each saw-tooth demarcates the edge of a convective roll. The formation of a convective roll could best be observed in shallower layers where there is adequate coupling between the buoyancy and thermocapillary forces. The series of Figures 7a−e summarize our observations. In these experiments, the depth of the solution was larger than the one that gave the complete convective rolls. These deeper solutions magnified the fingering effect for a better visual effect. Figure 7a shows the development of a third convective torus (the first two have already been formed; the separation between the first and the second is clearly evident). Surface tension gradients pull the thin top skin forward with the bulk solution progressing forward

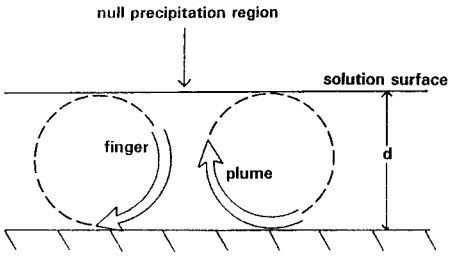

Figure 8. In comparison with Figure 5, faster-moving waves can produce separated convective rolls of the nature shown. Shown are two adjacent convective tori with a plume and a finger existing side-by-side; depriving the region between them of chemical reactivity. All convective tori spin in a clockwise direction. This is the situation obtaining in Figure 4.

by only reaction−diffusion and thermal convection forces. The red regions not only represent higher acid concentrations but also higher temperatures ($\Delta T \approx 2.8-4.5$ °C). The thin skin loses heat to the bulk solution faster than it can generate it (this happens the further it moves away from the bulk reacted region which is denoted by the red color). Since the reaction possesses a positive isothermal density change, this makes the tip of the leading front heavier than the bulk unreacted region as thermal equilibrium sets in. This results in fingering, and the leading front starts to sink as shown in Figure 7b,c. As the finger sinks into the unreacted region, it meets the resident back flow which sweeps the finger backward, toward the bulk reacted region (Figure 7d). This continues in Figure 7e until a region of unreacted solution is trapped between a forward flow at the top and a back flow at the bottom, completing a torus (Figure 7f). If viewed from the top, the area surrounding the unreacted region will appear lighter, while the surrounding areas will be darker.

Figure 8 shows a schematic diagram of the appearance of the concentric rolls. Studies using a microscope and polystyrene beads had shown that each band of null precipitation contains both a finger and a plume, thus leaving a region of unreacted material with no barium sulfate formation (nor acid formation when using methyl orange indicator). From Figure 5, it now becomes easy to understand the formation of thermal plumes: if the leading convective roll is not that far ahead of the trailing roll (as the wave propagation velocity decreases), the plume of the leading roll will emerge through the trailing roll, giving a thermal plume behind the wave front.

Discussion

Pattern formation has mainly been confined to isothermal systems. Nonisothermal systems studied so far involve buoyancy-driven Rayleigh−Benard convection.[30] However, the work of Smith[31] and Nield[32] has shown that surface tension can be a very powerful propagating force capable of producing periodic structures and standing waves. Spatiotemporal structures of hydrothermal waves have already been observed for fluids subjected to lateral heating.[33] When the temperature exceeds a certain critical value, hydrothermal waves traveling downstream can be observed. Without convection, the chemical systems studied in this manuscript would not show a lateral instability. At least cubic autocatalysis is necessary for a lateral instability, while the chlorite−thiourea and related reactions only display quadratic autocatalysis.[34] There are a number of forces responsible for the observed pattern formation in these reaction systems: diffusion; convection; advection; reaction. The propagation velocities observed for these chemical systems are about

100× faster than those observed for isothermal reaction−diffusion systems such that pure reaction−diffusion forces can be neglected at these time scales.

Effect of Convection. Chemical waves generated in an exothermic or endothermic reaction produce density inhomogeneities in the reaction medium.

$$\rho = f(T, c_i) \tag{3}$$

where ρ is the density of solution, T is the absolute temperature, and c_i represents the species concentration. The density will thus vary depending upon the extent of reaction and the temperature. The density, ρ, can then be derived from[35]

$$\rho = \rho_0(1 - \alpha(T - T_0) + \Sigma\beta_i(c - c_0) \tag{4}$$

where

$$\alpha = -(1/\rho)\delta\rho/\delta T \quad \beta = (1/\rho)\delta\rho/\delta c_i \tag{5}$$

with subscripts "0" denoting initial conditions. The first term in eq 4 represents the temperature dependence of density, and the second term, the concentration dependence. These two terms deliver opposite effects, which give rise to the observed multicomponent convection (fingering regime). At isothermal conditions, the first term vanishes, leaving only the second term which gives, in this reaction system, $\rho > \rho_0$. This inequality will dictate the effect of buoyancy at thermal equilibrium. However, for both reactants and products, the buoyancy factors can be estimated by the Grashof number:[36]

$$Gr = -(\delta\rho/\delta T)g\Delta T d^3/\rho\kappa\nu = \alpha g\Delta T d^3/\kappa\nu \tag{6}$$

Here d is the depth of the solution, κ is the thermal diffusivity, and ν is the kinematic viscosity. Our experiments evaluated $\delta\rho/\delta T = -0.4$ kg m^{-3} K^{-1} such that when $T > T_0$, the first term in eq 4 will pull the value of ρ to lighter values. With d raised to the third power, buoyancy factors will be much more pronounced in deeper fluid solutions. Hence the observed extensive fingering is observed in tube experiments.

Marangoni Convection. Table 1 shows the experimentally determined surface tension values for the chlorite−thiourea reaction. At isothermal conditions, the product solution has a slightly lower surface tension than the reactant solution. Thus, both reaction−diffusion and thermocapillary convection act in the same direction with respect to wave propagation.

$$\sigma = \sigma_0 - \tau(T - T_0) \tag{7}$$

with $\sigma =$ to surface tention and $\tau = (\delta\sigma/\delta T)_{P,c}$

Surface tension, in general, decreases with temperature, and our reaction solutions gave $\tau = -9.5 \times 10^{-5}$ N m^{-1} K^{-1}. Thermocapillary forces can be estimated from the Marangoni number, *Ma*:[37]

$$Ma = -\tau\Delta T l/\rho\nu\kappa$$

Here l is the length of the free surface. Although ΔT changes over a reaction zone of about 3 mm, a reasonable Marangoni number can be calculated from our experimental data. The Bond number,

$$B_0 = Ra/Ma \tag{8}$$

where *Ra* (Rayleigh number) = G$r\nu/\kappa$ is a better measure of the relative strengths of the forces responsible for the formation of the convective torus. In general, we calculate that the Bond number has a temperature-independent value of 0.40 for the same vessel and same conditions.[38] Numerical analysis of the strongly convective thermocapillary flows have shown that a finite temperature gradient remains over the entire free surface, leading to a global flow structure. This means that, for the same temperature gradient, the Marangoni effect is 2.5 times larger than the thermogravitational-based Rayleigh effects. We expect, theoretically, a strong dominance of thermocapillary effects over thermogravitational effects, and this was also observed experimentally in a previous publication from our laboratories.[12] It is thus easy to investigate our pseudo-two-dimensional thermocapillary-buoyancy flows. Theoretical work by Bergman and Ramadhyani[39] also concluded that thermocapillary convection dominates in such cavity problems in the limit of fixed B_0 and as $Ma \rightarrow \infty$.

From Fingering to a Plume. The formation of a finger is not based solely on the rapid heat exchange of the fingering region with the unreacted solution, thus rendering it heavier. One of the most important driving forces is the availability of reagents below it. Figures 3, 4, 6, and 7 show that there is a resident back flow at the bottom of the solution to compensate for the flow at the surface which is fueled by thermocapillary convection. So, as the finger proceeds down the solution, it is swept back wards, toward the unreacted (and reacting) solution. On reaching the bottom of the vessel, however, the reacting solution, which is already under a constant flow backward, has no choice but to curl upward behind the finger. Availability of reagents, again, give it only the choice to go upward. Due to the positive isothermal density changes observed with these chemical systems, plumes will travel upward at a speed slower than the finger travels downward. Careful examination of Figure 5 shows that, for thermal plumes, the path is into the reacting (and reacted) hot region behind it. So, the velocity of such plumes upward is much faster than what one might observe in Figure 2.

Conclusion

The majority of the theoretical work that predicts the type of flows and coherence reported in this manuscript relate to nonreacting media where the geometry of the cavity is fixed. The Benard−Marangoni instability with lateral heating, as elegantly presented by Villiers and Platten, also involves a pure fluid.[40] The involvement of chemical kinetics and a constantly moving boundary as presented by our traveling wave would have been supposed to render an already complex problem intractable. However, the dominance of the Marangoni effect in shallow layers allows for the study of the system by utilizing only the thermocapillary convection and ignoring the reaction−diffusion propagative forces. Theoretically, the absence of a reflection symmetry and the location of a driving force at the free surface increases the complexity of the Benard−Marangoni instability. However, theoretical work shows that when the free surface is undeformable, stationary convection develops with a finite average wavelength.[41] The convective tori observed in our system appear to represent stationary waves arising from a system with a freely deformable upper layer. Very few studies of hydrothermal waves have been performed in rectangular vessels; most studies are in cylindrical geometries.[37] By assuming a sharp temperature gradient at the wave front as well as an unbound horizontal plane, our chemical system can be reduced to the Villiers and Platten model. When it is reduced to this form, one can thus justify the observation of convective rolls.

Acknowledgment. Most of the write-up and data analysis for this manuscript was performed while R.H.S. was on sabbatical leave at the University of Cape Town and as visiting professor at the University of Natal-Durban campus. R.H.S. thanks both Chemistry Departments at UCT and UND for hosting him. This work was supported by Research Grant No. CHE 9632592.

References and Notes

(1) Part 5 (of 10) in the series of publications dedicated to the memory of Dr. Cordelia Rangarirayi Chinake, 1965−1998. Part 4: Oxyhalogen−Sulfur Chemistry: Oxidation of a Bunte Salt. *Phys. Chem. Chem. Phys*. **2001**, *3*, 4957.

(2) Turing, A. M. *Philos. Trans. R. Soc. London B* **1952**, *37*, 237.

(3) Cross, M. C.; Hohenberg, P. C. *Rev. Mod. Phys.* **1993**, *65*, 851.

(4) Castets, V.; Dulos, E.; Boissonade, J.; De Kepper, P. *Phys. Rev. Lett.* **1990**, *64*, 2953.

(5) Fecher, F.; Strasser, P.; Eiswirth, M.; Schneider, F. W.; Munster, A. F. *Chem. Phys. Lett.* **1999**, *313*, 205.

(6) Middya, U.; Luss, D.; Sheintuch, M. *J. Chem. Phys.* **1994**, *100*, 3568.

(7) Rotemund, H. H.; Jakubith, S.; Von Oertzen, A.; Ertl, G. *J. Chem. Phys.* **1989**, *91*, 4942.

(8) Lev, O.; Sheintuch, M.; Pismen, L. M.; Yamitzky, C. *Nature* **1988**, *336*, 458.

(9) Diewald, M.; Brand, H. R. *Phys. Rev. E* **1995**, *51*, 5200.

(10) Matthiessen, K.; Wilke, H.; Muller, S. C. *Phys. Rev. E* **1996**, *53*, 6056.

(11) Agladze, K.; Dulos, E.; De Kepper, P. *J. Phys. Chem.* **1992**, *96*, 2400.

(12) Martincigh, B. S.; Chinake, C. R.; Howes, T.; Simoyi, R. H. *Phys. Rev. E* **1997**, *55*, 7299.

(13) Chinake, C. R.; Simoyi, R. H. *J. Phys. Chem.* **1993**, *97*, 11569.

(14) Epstein, I. R.; Kustin, K.; Simoyi, R. H. *J. Phys. Chem.* **1992**, *96*, 5852.

(15) Jones, J. B.; Chinake, C. R.; Simoyi, R. H. *J. Phys. Chem.* **1995**, *99*, 1523.

(16) Simoyi, R. H.; Masere, J.; Muzimbaranda, C.; Manyonda, M.; Dube, S. *Int. J. Chem.. Kinet.* **1991**, *23*, 419.

(17) Chinake, C. R.; Simoyi, R. H. *J. Phys. Chem.* **1994**, *98*, 4012.

(18) Gy. Rabai Orban, M. *J. Phys. Chem.* **1993**, *97*, 5935.

(19) Taube, H.; Dodgen, H. *J. Am. Chem. Soc.* **1949**, *71*, 3330.

(20) Indelli, A. J. *J. Phys. Chem.* **1964**, *68*, 3027.

(21) Kern, D.; Kim, C.-H. *J. Am. Chem. Soc.* **1965**, *87*, 5309.

(22) Shoemaker, D. P.; Garland, C. W.; Nibler, J. W. *Experiments in Physical Chemistry*, 6th ed.; McGraw-Hill: New York; pp 291−300.

(23) Hulpert, H. E.; Turner, J. S. *J. Fluid Mech.* **1981**, *106*, 299.

(24) Ezersky, A. B.; Garcimartin, A.; Mancini, H. C.; Perez-Garcia, C. *Phys. Rev. E* **1993**, *48*, 4414.

(25) Martincigh, B. S.; Simoyi, R. H. *Phys. Rev. E* **1995**, *52*, 1606.

(26) Hauser, M. J. B.; Simoyi, R. H. *Chem. Phys. Lett.* **1994**, *227*, 593.

(27) Hauser, M. J. B.; Simoyi, R. H. *Phys. Lett. A* **1994**, *191*, 31.

(28) Chinake, C. R.; Simoyi, R. H. *J. Chem. Soc., Faraday Trans.* **1997**, *93*, 1345.

(29) Martincigh, B. S.; Hauser, M. J. B.; Simoyi, R. H. *Phys. Rev. E* **1995**, *52*, 6106.

(30) Bérnard, H. *Rev. Gen. Sci. Pure Appl.* **1900**, *11*, 1261.

(31) Smith, K. A. *J. Fluid Mech.* **1966**, *24*, 401.

(32) Nield, D. A. *J. Fluid Mech.* **1964**, *19*, 341.

(33) Gill, A. E. *J. Fluid Mech.* **1966**, *26*, 515.

(34) Horvath, D.; Petrov, V.; Scott, S. K.; Showalter, K. *J. Phys. Chem.* **1992**, *96*, 5852.

(35) Pojman, J. A.; Epstein, I. R. *J. Phys. Chem.* **1990**, *94*, 4966.

(36) Smith, M. K.; Davis, S. H. *J. Fluid Mech.* **1983**, *132*, 145.

(37) Char, M.-F.; Chiang, K.-T. *J. Phys. D* **1994**, *27*, 748.

(38) Nitschke, K.; Thess, A. *Phys. Rev. E* **1995**, *52*, 5772.

(39) Villiers, D.; Platten, J. K. *J. Fluid Mech.* **1992**, *234*, 487.

(40) Smith, M. K.; Davis, S. H. *J. Fluid Mech.* **1983**, *132*, 119.

(41) Lücke, M.; Mihelcic, M.; Kowalski, B. *Phys. Rev. A* **1997**, *35*, 4001.